Thresholds in road network functioning on US Atlantic and Gulf barrier islands

Sofia Aldabet[1], Evan B. Goldstein[2*], Eli D. Lazarus[1*]

[1]Environmental Dynamics Lab, School of Geography and Environmental Science, University of Southampton, Southampton, SO17 1BJ, UK

[2]Department of Geography, Environment, and Sustainability, University of North Carolina at Greensboro, Greensboro, NC, USA

**Corresponding Authors:* EBG: ebgoldst@uncg.edu / @ebgoldstein; EDL: e.d.lazarus@soton.ac.uk / @envidynxlab

ORCiDs:

SA: 0000-0002-6822-8330
EBG: 0000-0001-9358-1016
EDL: 0000-0003-2404-9661

Keywords – barrier island, development, flooding, network analysis, network robustness, road network

Key points

1) Living on barrier islands depends on functioning road networks, which are highly exposed to coastal hazard impacts
2) Road networks of US barrier islands have a range of network failure thresholds derived from elevation and annual exceedance probability
3) Thresholds in road network functioning can be incorporated into forward-looking models of barrier dynamics

Abstract

Barrier islands predominate the Atlantic and Gulf coastlines of the USA, where development exceeds national trends. Forward-looking models of barrier island dynamics often include feedbacks with management practices – particularly those aimed at mitigating damage to buildings from natural hazards – and how real estate markets may be linked to barrier island dynamics. However, models thus far do not account for networks of infrastructure, such as roads, and how the functioning of infrastructure networks might influence management strategies. Understanding infrastructure networks on barrier islands is an essential step toward improved insight and foresight into the future dynamics of human-altered barriers. Here, we examine thresholds in the functioning of 72 US Atlantic and Gulf Coast barrier islands. We use digital elevation models to assign an elevation to each intersection in each road network. From each road network we sequentially remove intersections, starting from the lowest elevation. In each network we identify a critical intersection – and corresponding elevation – at which the functioning of the network fails, and we match the elevation of each critical intersection to local annual exceedance probabilities for extreme high-water levels. We find a range of failure thresholds for barrier island road network functioning, and also find that no single metric – absolute elevation, annual exceedance probability, or a quantitative metric of robustness – sufficiently ranks the susceptibility of barrier road networks to failure. Future work can incorporate thresholds for road network into forward-looking models of barrier island dynamics that include hazard-mitigation practices for protecting infrastructure.

Plain Language Summary

Barrier islands are popular places to live and visit. To navigate barrier islands, people depend on extensive road networks. But barrier islands are especially exposed to impacts from hazards like storms, flooding, and sea-level rise. We use tools from network science to investigate how barrier island road networks might be disrupted by coastal hazards such as flooding (and other related hazards like road damage from flood water, and debris/sand accumulation). To do this we find the elevation of each intersection in each road network on 72 US Atlantic and Gulf barrier islands, and then track what happens to the network as we remove intersections, one at a time, starting with those at the lowest elevations. This process reveals the specific intersection at which a given network fails. We then link the elevation of that intersection to the likelihood of flooding from extreme high-water levels, which enables us to estimate whether a network might fail often or only rarely. Knowing the locations of these specific intersections in barrier island road networks could improve model forecasts of how barrier environments may evolve in the future, and inform coastal management and planning strategies for adaptation to changing coastal hazards.

1 Introduction

Barrier islands predominate the Atlantic and Gulf coastlines of the USA (Mulhern et al., 2017; Stutz & Pilkey, 2011). An estimated 4300–4700 km of open coast is parceled into as many as 282 islands (Dolan et al. 1980; Mulhern et al., 2017, 2021; Stutz & Pilkey, 2011), of which approximately a quarter have been described as "urbanized" (Dolan & Lins, 2000; Dolan et al. 1980). These host more than 1.4 million permanent residents (Zhang & Leatherman, 2011) and a disproportionate number of high-value properties (Nordstrom, 2004). Over recent decades, development of the built environment on US barrier islands has continued at rates that exceed national trends (McNamara & Lazarus, 2018; NOAA, 2013; Stutz & Pilkey, 2011; Zhang & Leatherman, 2011), unchecked by damaging impacts of large storms (Goldschalk et al., 1989; Lazarus et al., 2018).

The future dynamics of "urbanized" barrier islands will be determined by their built environments, and the persistence of localized hazard-mitigation practices (e.g., seawalls, breakwaters, groynes, beach nourishment, dune construction) to protect against storm impacts, chronic erosion, and sea-level rise (Armstrong & Lazarus, 2019; Lazarus & Goldstein, 2019; Lazarus et al., 2016, 2021; McNamara & Keeler, 2013; McNamara & Lazarus, 2018; McNamara & Werner, 2008a, 2008b; McNamara et al., 2015; Miselis & Lorenzo-Trueba, 2017; Nordstrom, 1994, 2004; Rogers et al., 2015). Construction and protection of the built environment in barrier settings alters natural pathways of sediment transport, which in turn redistributes and reapportions local sediment budgets (Nordstrom, 1994, 2004). Changes in the sediment budget in turn change spatial patterns of hazard exposure, to which coastal management and planning must respond. Research into this feedback, which has come to typify human-altered coastlines, has tended to emphasize the comparative morphological state of the barrier environment (McNamara and Werner, 2008a, 2008b) or to focus on the economic dynamics reflected in real-estate and property values (Armstrong et al., 2016; Armstrong & Lazarus, 2019; Gopalakrishnan et al., 2011, 2016; Lazarus et al., 2016; McNamara et al., 2011, 2015; McNamara & Keeler, 2013; McNamara & Lazarus, 2018; Smith et al., 2009; Williams et al., 2013). Much of this work uses numerical modelling to explore and understand potential thresholds in the human–environmental system that might drive barriers toward different management regimes – or even abandonment. However, subsumed in the spatial domains of these modelling exercises, but not addressed directly, are the networks of critical infrastructure – roads and public utilities – that are fundamental to the fabric of built environments. These networks connect physical spaces, with their own thresholds in functioning where failure may be abrupt.

Investigating infrastructure networks on developed barrier islands for thresholds in functioning – which could necessitate changes in management and planning – is an essential step toward improved insight and foresight into how human-altered barriers may evolve in the future. The analysis we present here examines potential thresholds in the functioning of US Atlantic and Gulf barrier island road networks. In the US, road networks tend to be the principal way in which people and goods reach and move within developed barrier islands, and are vital to hazard evacuation, emergency response, and recovery operations during and after catastrophic storms (Anarde et al., 2018; Darestani et al., 2021; Godschalk et al., 1989; Frazier et al., 2013; Velasquez-Montoya et al., 2021). Road network disruptions – mechanisms that cause reductions in mobility or increases in the costs necessary to maintain the desired levels of mobility (Markolf et al., 2019) – are common on barrier islands during hurricanes, tropical storms, and nor'easters (Dolan & Lins, 2000; Hardin et al., 2012; Krynock et al., 2005; Nordstrom, 2004; Nordstrom & Jackson, 1995; Spanger-Siegfried et al., 2014; Velasquez-Montoya et al., 2021), and also occur as a result of king tides, sea-level anomalies, groundwater flooding, or other factors that lead to nuisance or "sunny day" flooding (Fant et al., 2021; Hino et al., 2019; Housego et al., 2021; Jacobs et al., 2018; Moftakhari et al., 2015, 2017, 2018; Praharaj et al., 2021). Road disruptions can lead to major socio-economic impacts, isolating neighborhoods, compromising evacuation, and preventing people from accessing critical services (Balomenos et al., 2019; Dong et al., 2020a; Jenelius & Mattson, 2012; Spanger-Siegfried et al., 2014; Suarez et al., 2005). The maintenance and restoration of other critical systems – electricity, water supply, communications – often depends on a functioning road system (Chang, 2016; Johansen and Tien, 2018; Mattson & Jenelius, 2015; Nicholson & Du, 1997).

Because road systems are networks, they can be investigated with the quantitative tools of graph theory (Albert & Barabási, 2002; Boeing, 2017, 2019, 2020; Callaway et al., 2000; Holme et al., 2002; Iyler et al., 2013; Jamakovic and Uhlig, 2008; Kirkley et al., 2018; Moriera et al., 2009; Porta et al., 2006; Tian et al., 2018). Note that network analyses have also been variously applied to coastal morphology and dynamics in non-built environments (Hiatt et al., 2021; Passalacqua, 2017; Pearson et al., 2020; Tejedor et al., 2018). Within the large and rapidly expanding body of research into climate-driven disruptions to critical infrastructure (Faturechi & Miller-Hooks, 2014; Jaroszweski et al., 2014; Markolf et al., 2019; Neumann et al., 2021; Wang et al., 2020), a subset is exploring specifically the exposure and susceptibility of infrastructure to different drivers of flood disturbance. Studies consider road and other transportation networks in urban coastal settings (de Bruijn et al., 2019; Kaskalmar et al., 2020; Kermanshah & Derrible, 2017; Plane et al., 2019; Rotzoll & Fletcher, 2013; Suarez et al., 2005; Sweet et al., 2014; Pezza &

White, 2021) and in fluvial floodplains and upland catchments (Abdulla & Birgisson, 2021; Arrighi et al., 2021; Dave et al., 2021; Dong et al., 2020a; Evans et al., 2020; Kelleher & McPhillips, 2020; Pregnolato et al., 2017; Singh et al., 2018; Versini et al., 2010; Wang et al., 2019); others focus on water-treatment systems in low-lying coastal regions (Hummel et al., 2018) or multiple layers of infrastructure networks (Douglas et al., 2016; Habel et al. 2017, 2020; Koks et al., 2019; Neumann et al., 2021).

Here, we examine the drivable road networks of 72 barrier islands along the Atlantic and Gulf Coasts of the USA (**Fig. 1**), selected because their networks contain >100 nodes. First, we cast the road network of each barrier island as a separate graph of nodes (intersections) connected by edges (road segments). We use spatially extensive digital elevation models to assign an elevation to each node (intersection) in each road network. For each barrier island, we sequentially remove nodes from the network, starting from the lowest elevation, and identify the critical node – with its corresponding elevation – at which each barrier island road network crosses a threshold of functioning. We then link the elevation of each critical node to the local annual exceedance probability curve for extreme high-water levels. Our analysis demonstrates a method to identify specific physical locations that, if disrupted by flooding or a flood-related hazard (e.g., road damage, debris/sediment accumulation), could trigger functional failure in an island road network. We organize the components of this threshold, which varies by barrier island, in terms of common metrics – elevation and annual exceedance probabilities – to facilitate their incorporation into forward-looking modeling of developed barrier island dynamics.

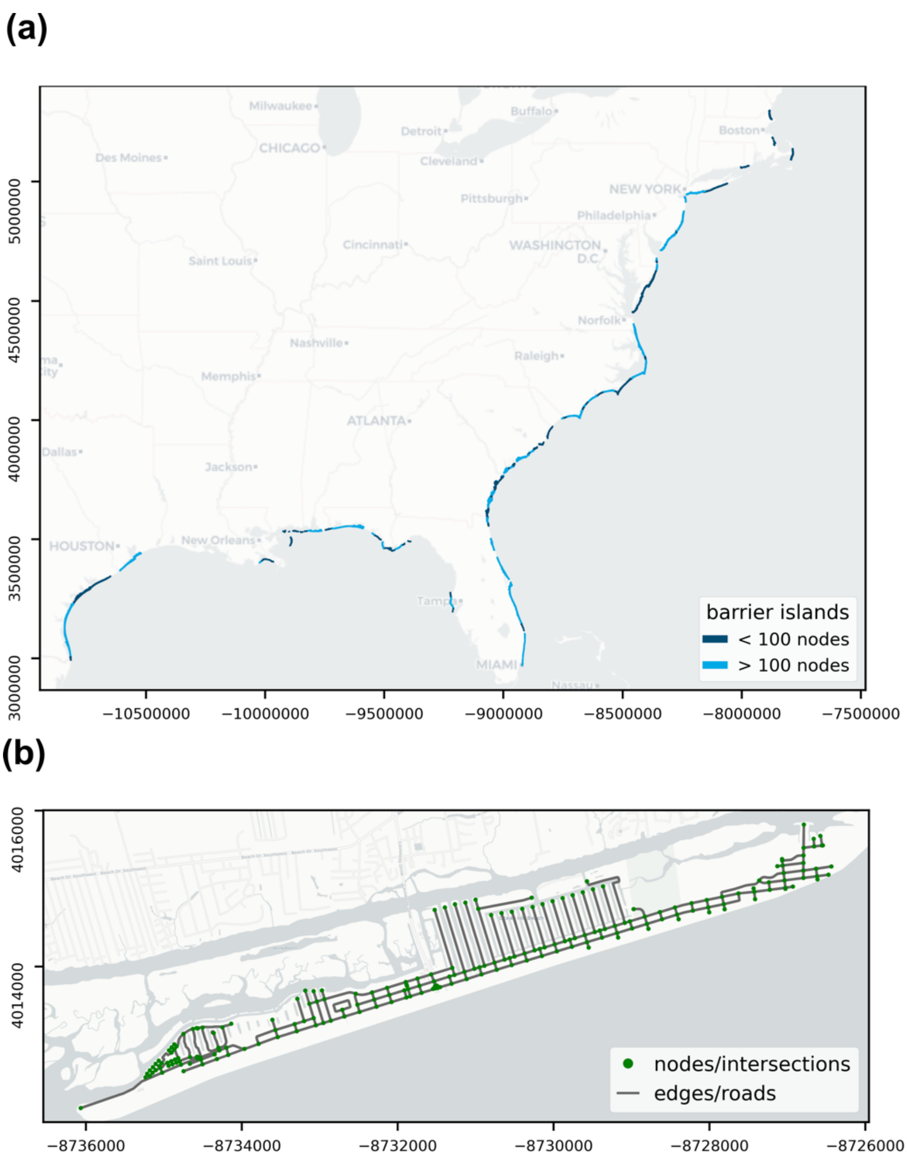

Figure 1. *US Atlantic and Gulf Coast barrier islands considered in this study, and their road networks.* **(a)** *Map of 184 barrier islands (Mulhern et al., 2017, 2021), of which 74 have road networks with >100 nodes (intersections). Of those, 72 (light blue) overlap with tiles currently available in the Continuously Updated Digital Elevation Model data from NOAA (Amante et al., 2021; CIRES, 2014).* **(b)** *Example of drivable road network at Ocean Isle, North Carolina, USA, in which intersections are represented as nodes and roads as edges. Maps shown in Web Mercator projection (EPSG:3857).*

2 Methods

Our workflow for investigating US Atlantic and Gulf barrier island road networks is shown in **Fig. 2**. We discuss each step in the sequence below.

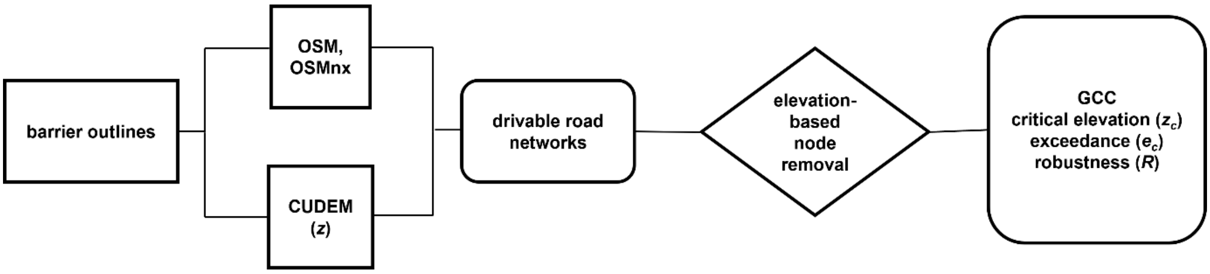

Figure 2. *Methodological workflow for assessing robustness to flood-induced failures in road networks on US Atlantic and Gulf barrier islands. Abbreviations are as follows: OSM is Open Street Map; OSMnx is an analytical toolbox (Boeing, 2017). CUDEM is the NOAA Continuously Updated Digital Elevation Model (Amante et al., 2021; CIRES, 2014). GCC is the giant-connected component of a network, or the large cluster of nodes connected in the original network.*

2.1 Road networks and topography

To isolate barrier island road networks, we used digitized perimeters of 184 barrier islands along the Atlantic and Gulf Coasts of the USA as spatial boundaries (Mulhern et al., 2017, 2021) and extracted the drivable road networks from Open Street Map (OSM) with OSMnx (Boeing, 2017). Cast as networks, road intersections are encoded as nodes and road segments are edges. We excluded other possible transportation pathways such as bikeways and walkways.

Of the 184 barriers considered, 108 have drivable road networks, according to their classification within OSM. Of those, 103 overlapped with tiles currently available in the NOAA Continuously Updated Digital Elevation Model (CUDEM), a set of 1/9 Arc-Second resolution bathymetric and topographic tiles for the coastal USA (Amante et al., 2021; CIRES, 2014). Note that some of these 103 networks are sandy tracks or access roads, or networks with very few nodes. For statistically meaningful metrics of network structure, we restricted our analysis to barriers with drivable road networks of at least 100 nodes (**Fig. 1**). This reduced our sample to 72 barriers. We determined the elevation of each node (road intersection) in each network by spatially querying the CUDEM dataset.

The size of this subset is broadly consistent – despite very different selection criteria – with the count by Dolan et al. (1980), who identified 70 barrier islands as "urbanized". We did not attempt to reconcile differences in reported numbers of US Atlantic and Gulf barrier islands: Dolan et al. (1980) report 282 islands; Stutz and Pilkey (2011) report 277; Mulhern et al. (2017, 2021) digitized 184. Note that several developed barrier islands are missing from Mulhern et al.

(2017), but we use this dataset from Mulhern et al. (2017, 2021) because it is the only barrier compilation that is openly accessible.

2.2 Network response to node removal

The susceptibility of a network to the failure of its components is typically explored by nullifying or removing nodes and calculating metrics that reflect network functioning (Abdulla & Birgisson, 2021; Iyer et al., 2013; Li et al., 2015; Newman, 2010; Schneider et al., 2011; Wang et al., 2019). For example, when enough of the network is removed, travel between any two nodes (intersections) becomes impossible or requires long travel distances (and time) on the network. We removed nodes from a network based on a ranked list by elevation – from lowest to highest – in contrast to removing nodes randomly (a common approach, e.g., Albert & Barabási, 2002). Node removal in this way mimics a simplified "bathtub" flooding scenario (e.g., Abdulla & Birgisson, 2020; Wang et al., 2019), which assumes that nodes become nullified because they are actively flooded, damaged by flooding, and/or unusable because of debris and/or sand deposited on the road. We assumed that the removal of a node causes the immediate disconnection of all its connected edges. This work thus considered node removal exclusively; edge removal could also be explored, with the inclusion of other contextual physical metrics such as road grade, lowest street elevation, or average street elevation. Network metrics were calculated using NetworkX (Hagberg et al., 2008).

For road networks, the original network is connected in a single large cluster – the giant-connected component (or giant component). As nodes in the original network are serially removed, the network breaks into smaller networks. Here, we tracked the size of these subnetworks relative to the size of the giant component. Specifically, as the fraction of nodes removed (q) increases and the first giant component degrades, we tracked the size of the second-largest cluster – the second giant connected component (**Fig. 3a**). The network crosses a critical threshold at q_c, when the first giant component fragments and the size of the second giant component becomes maximal (Li et al., 2015; Wang et al., 2019). Generally, the higher q_c – that is, the more nodes that can be removed before the giant component fragments – the less prone the network is to failure (Newman, 2010). The critical threshold (q_c) can be linked to a specific node that causes the failure of the network (**Fig. 3b**) and to the elevation of that node, which we refer to as the critical elevation (z_c).

2.3 Extreme water levels

Comparison of coastal barrier islands solely on the basis of topographic elevation (i.e, one barrier is higher or lower than another) is not meaningful unto itself because of local differences in tidal forcing and extreme water level statistics. For example, road networks on higher-standing barriers subject to frequent extreme storms might be more prone to flooding than road networks on lower-lying barriers subject to fewer storms. To provide meaningful comparisons among the broad geospatial distribution of barriers in our sample, we recast all node (intersection) elevations to local annual exceedance probabilities of extreme water events.

Extreme water levels have been used to examine the direct and indirect impacts of coastal floods on transportation systems and assess the susceptibility of the network to flood-induced failure (Fant et al. 2021; Habel et al., 2020; Jacobs et al., 2018; Pezza & White, 2021). Annual exceedance probabilities and average recurrence intervals are commonly applied for infrastructure design and assessment of flood risk (Apel et al., 2004, 2006; Hackl et al., 2018; Haigh et al., 2014; Sweet & Park, 2014; Vitousek et al., 2017; Wahl et al., 2017). Average recurrence intervals, also known as return periods, provide an estimation of the time elapsed between events of the same magnitude; annual exceedance probability refers to the likelihood that high-water levels exceed a certain elevation in any given year (Haigh et al., 2014). For example, a flood with an annual exceedance probability of 0.01 corresponds to an event that has a 1% chance of annual occurrence, or an average recurrence interval of 100 years. (Return period can be understood as the inverse of exceedance probability.)

Extreme value analysis (EVA) – the branch of statistics that deals with the estimation and prediction of rare values within a series (Coles, 2001) – has been applied broadly to analyses of observed and simulated extreme high-water levels to quantify the probability of occurrence (and/or return period) of extreme events (Vitousek et al., 2017; Wahl et al., 2017; Zervas, 2013). One of the most common EVA methods is block maxima, which considers the maximum of all recorded values within a block of time (i.e., days, months, or years) and approximates extreme values using a Generalized Extreme Value distribution (GEV) (Coles, 2001; Zervas, 2013). The GEV distribution is described by three parameters – location (μ), scale (σ), and shape (ξ) – that refer, respectively, to the center of the distribution, the deviation around the mean, and the tail behavior of the distribution. The shape parameter determines the extreme distribution used: Gumbel ($\xi = 0$), Frèchet ($\xi > 0$) or Weilbull ($\xi < 0$). Using long-term monthly tide gauge records from the 112 US stations operated by the Center for Operational Oceanographic Products and Services (CO-OPS), Zervas (2013) followed a GEV approach to characterize the distributions of extreme high and low-water levels and produce exceedance probability curves for each station. For each barrier island in this analysis, we generated extreme high-water level annual exceedance probability curves by sampling the Gumbel distribution described by the three reported GEV parameters (Zervas, 2013) for the tidal station closest to that barrier by straight-line distance. We then estimated annual exceedance probabilities for the critical node of each barrier network, which we refer to as the critical exceedance, e_c. We thus linked each critical node to a specific annual exceedance probability. All calculation was done using the Python ecosystem, e.g., Scipy (Virtanen et al., 2020) and Numpy (Harris et al., 2020). Note that the choice of extreme value analysis applied to a data set has the greatest effect on events with the lowest likelihood of occurrence (Wahl et al, 2017). Because high-likelihood events are of particular interest to us in this analysis, the Gumbel distributions that we use to reproduce the estimates reported by Zervas (2013) are sufficient: a different method of extreme value analysis would result in different probabilities for the low-likelihood events from these tide gauges, but estimates for high-likelihood events will be effectively the same.

2.4 Network robustness

Having focused on identifying a single critical node for each island and defining a critical threshold for each barrier road network in terms of elevation (and exceedance probability), we next examined the overall network robustness of each barrier. The purpose of this step is to provide a summary metric for network functioning that includes but is not limited to the occurrence of the critical threshold: for example, determining how much of the original road network is still connected when any given percentage of the nodes is removed. Calculating whole-network robustness permitted us to compare barrier road networks in terms of their entire architecture, rather than solely by comparing aspects of a single critical node (e.g., its elevation and the related exceedance value).

We used the robustness metric *R* proposed by Schneider et al. (2011), which measures the summed size of the giant-connected component as nodes are removed (**Fig. 3c**):

$$R = \frac{1}{N} \sum_{Q=1}^{N} s(Q) \qquad (1)$$

where N refers to the total number of nodes in the network, Q to the number of nodes removed and $s(Q)$ is the fraction of nodes in the giant component after removing Q nodes. The normalization factor $1/N$ allows comparison between networks of different sizes. The resulting R values range between $1/N$ (for a star graph) to 0.5 (a fully connected network; Schneider et al., 2011). Note that we evaluated network robustness in two ways: by removing nodes in rank order of elevation (lowest to highest) and by random node removal (e.g., Wang et al., 2019). Other studies have investigated how R changes with non-random but abstracted network disruptions (Iyer et al., 2013), and how R varies in transportation networks, specifically, with different types of disruptions (Dong et al., 2020b; Wang et al. 2019).

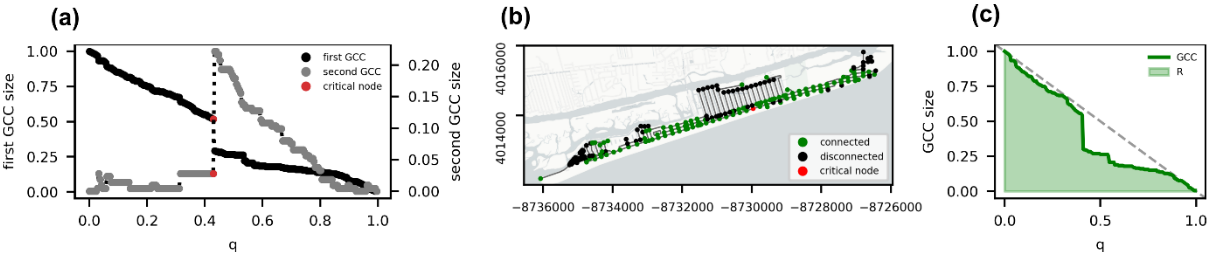

Figure 3. *Examples illustrating the methodology used to* **(a)** *explore the size decay of the first and second giant-connected components (GCC),* **(b)** *identify the critical node that leads to the fragmentation of the network, and* **(c)** *quantify overall network robustness to elevation-based node removal. Barrier example shown here is the drivable network at Ocean Isle, North Carolina, USA. In* **(a)***, the vertical axes show the first (left) and second (right) GCC size as a fraction of nodes in the original network, as a function of the fraction of nodes removed (q). Red dot in panels* **(a)** *and* **(b)** *marks the critical node in the GCC and in real physical space, respectively. In panel* **(c)***, robustness* R *is taken as the area (light green) under the decay curve for the first GCC (bold green). Dashed gray line shows the inverse 1:1 reference line, indicating the theoretical maximum for* R *= 0.5. Maps like the example shown in* **(b)** *for all 72 barrier road networks with >100 nodes can be found in the data repository.*

3 Results

3.1 Barrier island road networks

Of the 184 barrier islands considered in this analysis (Mulhern et al., 2017, 2021), 74 have drivable road networks with more than 100 nodes, and only 72 overlap with CUDEM tiles. These 72 islands account for 65% of the total US Atlantic and Gulf barrier island area (3,082 km^2 out of 4,716 km^2) and 60% of the US Atlantic and Gulf barrier island shoreline length (4,282 km out of 7,150 km) delineated in the dataset by Mulhern et al. (2017, 2021). On average, the 72 islands with networks of >100 nodes are typically three times larger (43 km^2) than barrier islands with small or no drivable road networks (15 km^2). Almost 90% of the 72 islands (63 barriers) are smaller than 100 km^2, and ~60% (42 barriers) have total area below 25 km^2 (**Fig. 4a**). Road network size is variable, ranging between 19 km and 678 km of total road length (143 km on average; **Fig. 4b**) and between 111 and 3486 intersections (739 nodes on average; **Fig. 4c**). Approximately 20% of these drivable networks (16 networks) have more than 200 km of total street length, and more than 25% (19 networks) have more than 1000 nodes. The average node elevation for the 72 road networks with >100 nodes is 2.5 m (**Fig. 4d**). Of all nodes in the dataset, ~65% sit between 1 and 3 m elevation (34,438 nodes out of 53,214), and ~8% (4,516 nodes) are below 1 m elevation. Conversely, barely 7% of all road intersections (3,695 nodes) are located above 5 m elevation, and only 0.5% (265 nodes) are above 10 m elevation.

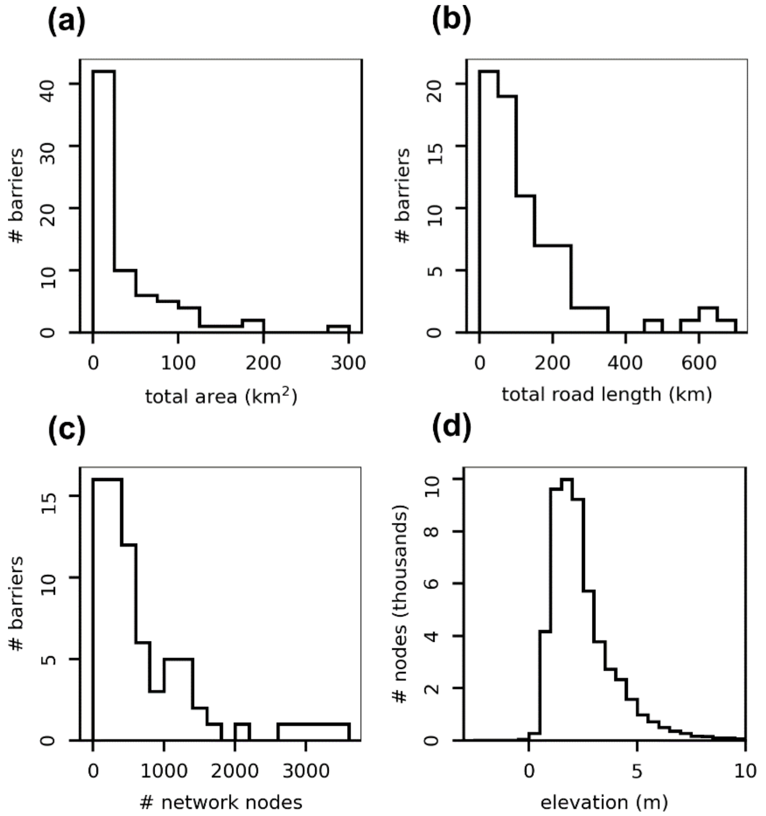

Figure 4. *Summary statistics for 72 US Atlantic and Gulf barrier-island road networks with >100 nodes. Panels show distributions of* **(a)** *total area,* **(b)** *total road length, and* **(c)** *the number of networked nodes for all 72 barriers. Panel* **(d)** *shows the distribution of elevation for all networked nodes in all 72 barriers.*

3.2 Elevation-based node removal

Elevation plays a primary role in determining the sequence of road closures, where intersections at the lowest elevations are expected to be among the first disrupted during floods (e.g., Abdulla and Birgisson, 2021): disruption might include being submerged by the flood, being physically damaged by flood water, and being buried under debris and/or sediment deposited by flooding. The aggregate compilation of all networked node elevations shows that most nodes sit below 5 m (**Fig. 4d**). We also plot each node in a given network in ranked order of elevation, from lowest to highest, for all 72 barriers with networks >100 nodes – a representation akin to a hypsometric curve (**Fig. 5a**) – which demonstrates the topographic similarity of these road networks despite the geographic distribution of the barriers on which they are situated. For each road network, we used the ranked order of node elevation to sequentially remove nodes, from lowest to highest, and plot the corresponding size of the first giant-connected component (**Fig. 5b**). We find that two general modes of behavior emerge. In one mode, the giant component decreases linearly with each node removed: as one node is removed from network, one node is removed from the giant component. This occurs as the removed nodes come from areas at the extremities of the network, or where the network is highly connected and nodes are linked by multiple edges (i.e., removal of a single intersection from a gridded network). In the other mode, the removal of a single node results in a sharp drop in giant component size. An example of this is the loss of a single node that links two parts of an island, each with its own cluster of nodes. Large, abrupt changes in the size of the giant component indicate the presence of nodes whose removal results in the fragmentation of the network. Thus, although these 72 barrier networks appear similar topographically, node removal on the basis of elevation does not yield identical curves because of differences in local network architecture (**Fig. 5b**).

We find that for all 72 road networks with >100 nodes, the elevation of the critical node (z_c) – the node whose removal from the network simultaneously reduces the size of the first giant component and maximizes the size of the second giant component – lies below 5 m (**Fig. 5c**). Moreover, 85% (61 networks) have critical nodes below 2.5 m; 44% (32 networks) have critical nodes below 1.5 m; and 18% (13 networks) have a critical node below 1 m. Unlike the more varied curves apparent when the size of the giant component is plotted as a function of the fraction of nodes removed (**Fig. 5b**), plotting the size of the giant component as a function of the elevation of each node removed emphasizes the precarity implied by such low elevations for critical nodes (**Fig. 5d**): the size of the giant component decays all but instantaneously as node elevation increases. However, similarly low-lying topography does not equate to similar likelihoods of flooding. For that, we needed to consider geographic differences in extreme water level.

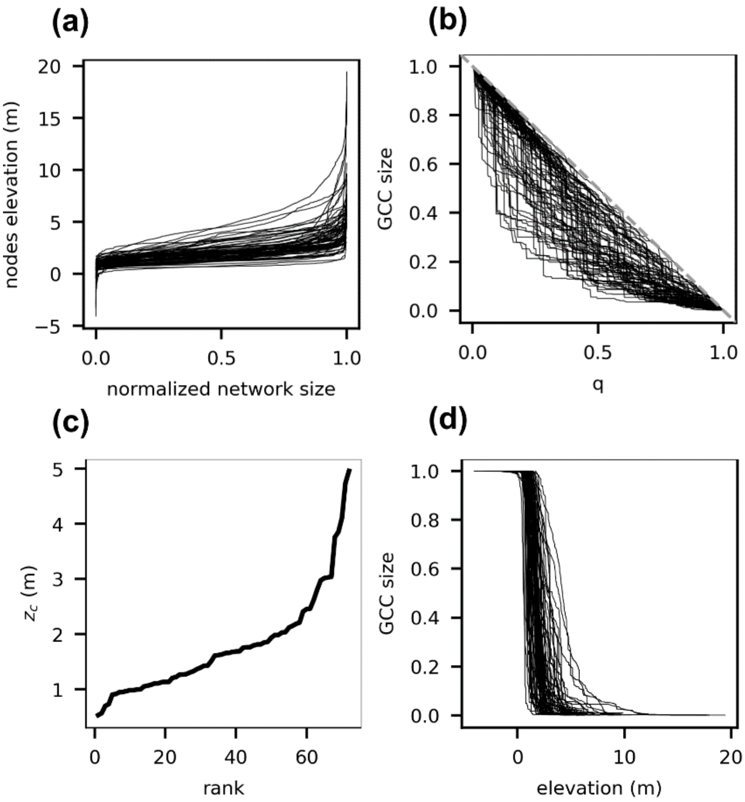

Figure 5. *Network effects of node removal based on ranked list of elevation (from low to high).* **(a)** *Elevation of each networked node, sorted into a ranked list from lowest to highest, for 72 barriers with networks with >100 nodes. Network size is normalized to 1.* **(b)** *Size decay of each giant-connected component under sequential node removal by elevation, from lowest to highest. Gray dashes are the inverse 1:1 reference line.* **(c)** *Elevation of the critical node (z_c) for each of the 72 road networks with >100 nodes, ranked from lowest to highest.* **(d)** *Size decay of each giant-connected component as a function of node elevation.*

3.3 Extreme water levels

Inferring road network susceptibility to failure purely in terms of node elevation is not meaningful. Tidal range varies along the US Atlantic and Gulf coastline, as does exposure to extreme high-water levels (i.e., hurricanes, nor'easters, and sea-level anomalies). We therefore connected each barrier road network node elevation to estimated local exceedance probabilities of extreme high-water levels. As a result, nodes at the same elevation but on different barrier islands can be associated with markedly different annual exceedance probabilities (**Fig. 6a**). We find that 44 of the 72 barrier networks (61%) have critical nodes at elevations associated with annual exceedance probabilities >0.01 (greater than 1% per year, or an average recurrence time of once every 100 years; **Fig. 6b**). Of those, 25 networks – over a third of the barriers sampled – yield critical thresholds in annual exceedance probability at or above 0.1 (10% chance per year, or an average recurrence time of once every 10 years). The critical elevation for those nodes is, on average, just above 1 m elevation (**Fig. 6c**). Generally, we find that local critical exceedance (*e_c*) is associated with the elevation of the critical node (*z_c*) (**Fig. 6c**).

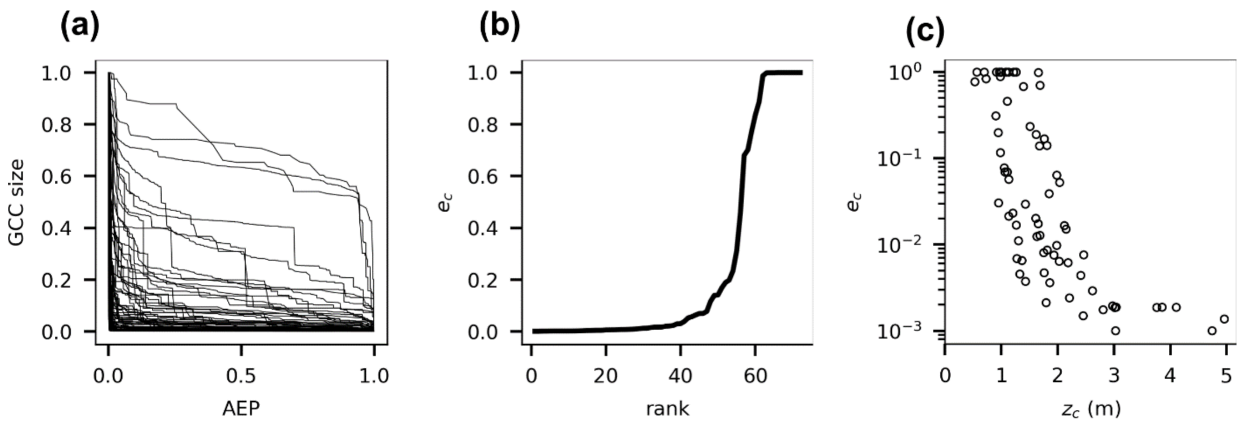

Figure 6. *Relationships between road networks and extreme water levels.* **(a)** *Size decay of the giant connected component versus annual exceedance probability (AEP) of extreme high-water events, based on the elevation of each node removed.* **(b)** *Barrier islands ranked according to exceedance probability of the critical node (e_c).* **(c)** *Relationship between the exceedance probability of the critical node for each barrier (e_c) as a function of the critical-node elevation (z_c).*

3.4 Road network robustness

We calculated road network robustness to measure the ability of the road network architecture to withstand node removal. Recall that robustness (*R*) is the normalized, summed size of the giant-connected component as nodes are removed (Eq. 1, after Schneider et al., 2011). We first focus on robustness by removing nodes in order of elevation (low to high). For the 72 barriers with networks >100 nodes, we show the giant component as a function of the fraction of nodes removed (as in **Fig. 5b**), now colored by the corresponding *R* value (**Fig. 7a**). When the size of the giant component decreases linearly with each successive node removed – as shown by the inverse 1:1 reference line (gray dashes) – the area under the curve is maximized, and so is the associated *R* value (*R* = 0.5). Color makes the gradient in *R* visually apparent: low values (purples) are associated with the farthest excursions from the 1:1 reference line, and high values (yellows) are concentrated closest to the reference line.

Approximately 35% of the networks (26 islands) have $R > 0.4$, with four networks above 0.45. Nearly half of the barriers analyzed (32 islands) fall within the range $0.3 < R < 0.4$, and the remaining 20% of the networks (14 islands) have R < 0.3, with one network below 0.2 (**Fig. 7b**). The highest R values in our sample illustrate behavior close to an end-member situation, where the giant component decreases almost linearly until nearly two-thirds of the nodes in the network are removed ($q_c \sim 0.6$) – at which point, the network begins to disintegrate (**Fig. 7c**). By contrast, networks with low R values are characterized by abrupt reductions in the size of the giant component with the removal of a small fraction of nodes (**Fig. 7d**).

Related work on flood-driven disruptions to road networks has demonstrated quantitative differences between the behavior of the giant component with preferential removal of nodes by elevation versus random node removal (Abdulla and Birgisson, 2021; Wang et al., 2019). We likewise show that a given network can have high robustness to elevation-based node removal, yet low robustness to a random node removal (**Fig. 7c**). Note that in some networks robustness values for elevation-based removal are low, and there is little difference between elevation-based removal versus random removal (**Fig. 7d**), suggesting an intrinsic low robustness in network architecture that is independent of removal order type.

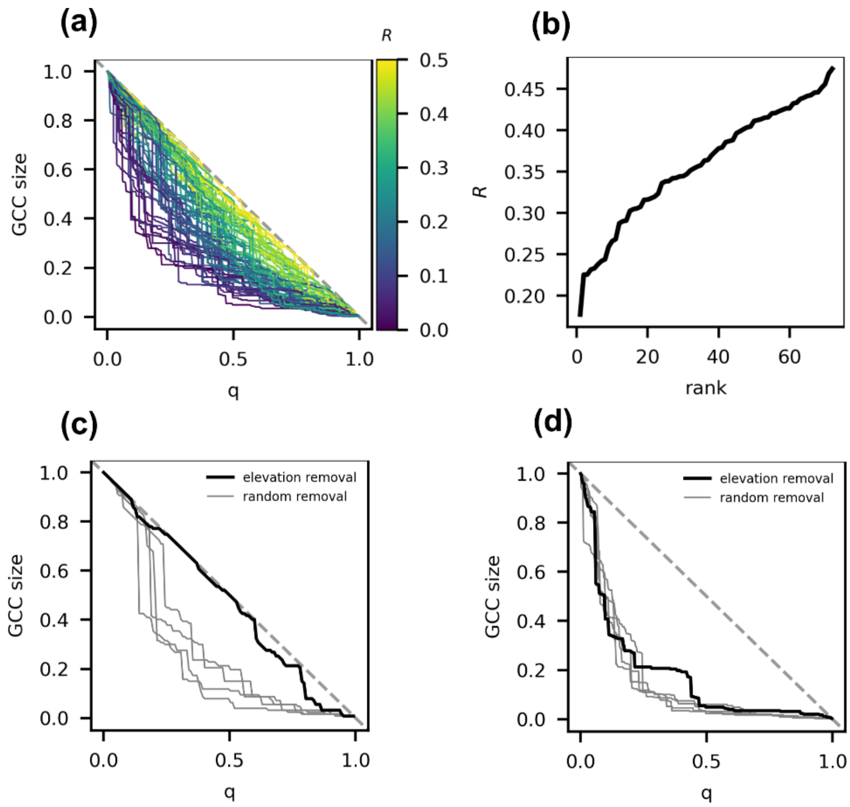

Figure 7. *Road network robustness.* **(a)** *Normalized giant-connected component size as a function of fraction of network nodes removed (as in Fig. 5b), where color represents values of robustness (purple ~ low; yellow ~ high). Dashed gray inverse 1:1 reference line denotes the curve for perfectly linear GCC decay with a theoretical maximum robustness of* R *= 0.5.* **(b)** *Rank-order plot of robustness values for the 72 barriers with >100 nodes.* **(c)** *Decay of giant component as a function of fraction of nodes removed for a network with high robustness to flooding disturbance (black line;* R *= 0.47; island FL28 in Mulhern et al. (2021)). Solid gray lines show comparatively distinct decay curves for the same network under random node removal.* **(d)** *Decay of giant component as a function of fraction of nodes removed for a network with low robustness to flooding disturbance (black line;* R *= 0.17; island SC1 in Mulhern et al. (2021)). Solid gray lines show similar decay curves for the same network under random node removal.*

4 Implications

4.1 No single metric can be used to rank barrier susceptibility to disruption

Taken together, the key variables explored in this work – critical node elevation (z_c), critical exceedance (e_c) and robustness (R) – provide a window into the complexity of elevation-based disturbance to road networks on seemingly similar barrier environments. Collating these three variables in a parallel-coordinates plot shows that the ranking of barriers changes depending on the metric (**Fig. 8**). Here, the barriers are first ranked by critical elevation (z_c) in ascending order (left column), then by critical annual exceedance probability (e_c) in descending order (middle column), and then by robustness (R) in ascending order (right column). The top of the plot thus uniformly corresponds to barrier networks that are less susceptible to disturbance based on each metric. Barrier islands are colored according to their elevation rank (sequence in first column), and each color tracks across the other two columns for e_c and R. Connecting lines cross as individual barriers change places in the respective rankings. This result illustrates a key insight: a barrier network might appear worryingly susceptible to disturbance on a ranked list according to one variable but reassuringly strong according to another. That is, a network might have a notably low critical node elevation, but be situated in a place unlikely to be affected by extreme high-water levels, and/or be characterized by an architecture with high robustness to elevation-controlled (i.e., flooding) disturbance. Cognate studies of hazard-driven disturbance to road networks have reached similar conclusions regarding the elusiveness of a single, definitive, ranking metric that captures network susceptibility to failure (Kermanshah & Derrible, 2016).

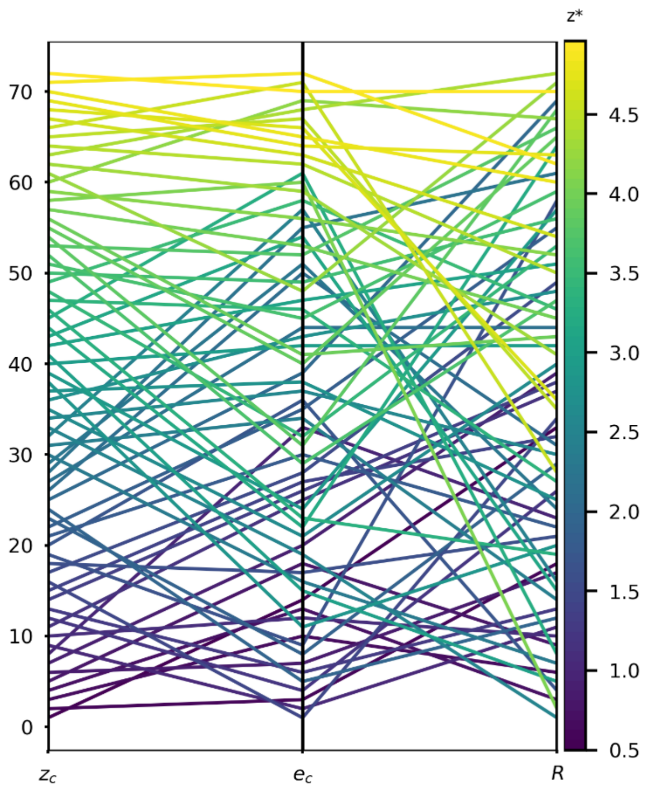

Figure 8. *Parallel-coordinates plot of critical node elevation* (z_c)*, exceedance probability* (e_c)*, and robustness* (R) *for barriers with road networks of >100 nodes. In each column, respectively, barriers (labeled at far left) are ranked by* z_c *in ascending order, by* e_c *in descending order, and by* R *in ascending order. Each barrier is colored by* z_c*, and that color follows each barrier across the plot as its relative rank changes for* e_c *and* R.

4.2 Caveats: non-stationarity and interdependencies in hazard forcing

Our analysis does not account for non-stationarity in environmental forcing, which is needed for work like this to be incorporated in future-looking modeling of barrier island dynamics. Our results are therefore indicative of road network robustness to disturbance on US Atlantic and Gulf barriers based on past conditions, but likely underestimate annual exceedance probabilities for critical nodes (e_c) in the future, as even high-likelihood events become more frequent. Future work should incorporate and explore the effects of forcing non-stationarity (e.g. Buchanan et al., 2017; Cheng & AghaKouchak, 2014; Ezer & Atkinson, 2014; Kirezci et al., 2020; Moftakhari et al., 2015; Sweet & Park, 2014; Taherkhani et al., 2020; Tebaldi et al., 2012; Vitousek et al., 2017; Wahl, 2017). We anticipate that the primary effect of non-stationarity would be to raise critical exceedance over time across the dataset, driving more barriers – some more rapidly than others – toward high if not guaranteed annual exceedance probabilities.

We also do not explicitly consider flood drivers or specific impacts of flooding (e.g., standing water, road damage, debris and sediment deposition), and instead focus on network disruption based purely on elevation. Future work can incorporate observations on how road networks are impacted by relative contributions of specific drivers from marine sources (Serafin et al., 2017) and others, such as pluvial (Dave et al., 2021; Evans et al., 2020; Kelleher & McPhillips, 2020; Neumann et al., 2021; Pregnolato et al., 2017) or groundwater flooding (Habel et al. 2017, 2020; Plane et al., 2019; Rotzoll & Fletcher, 2013), or the potential importance of variability in flood duration (Arrighi et al., 2021; Darestani et al., 2021; de Bruijn et al., 2019; Najibi & Devineni, 2018; Pezza & White, 2021; Sweet et al., 2014).

As empirical and modeled data for constructing annual exceedance probabilities for extreme high-water levels continue to improve (Muis et al., 2020; Tadesse & Wahl, 2020; Woodworth et al., 2017), so too will analyses of infrastructural robustness to flooding at specific localities – which might involve recalculating probabilities of infrastructural failure under non-stationary forcing (Cheng & AghaKouchak, 2014) and/or including the mitigating or exacerbating effects of coastal landscape morphodynamics (Anarde et al., 2018; Darestani et al., 2021; Velasquez-Montoya et al., 2021). Nevertheless, gaining insight into the probability distribution – and non-stationarity – of multi-source flood magnitude and frequency will also require a proliferation of accessible, comprehensive, multi-layer datasets (Habel et al., 2020). Emerging multi-layer datasets will not only include environmental forcings, but also different types of susceptible infrastructure

(Emanuelsson et al. 2014; Neumann et al., 2021), of which road networks are only one: recent works in this expanding research space consider wastewater treatment facilities (Hummel et al., 2018), storm-water conduits (Habel et al., 2020), rail and tunnel systems (Douglas et al., 2016; Koks et al., 2019), and interdependencies across multiple infrastructure systems (Najafi et al., 2021).

4.3 Identifying hotspots of concern

Our analysis offers a computationally efficient way of exploring (with open-access data sets) barrier island road network robustness to disturbance from extreme high-water events. The resulting isolation of a critical node associated with large-scale network failure is essentially a first-order diagnostic, derived from the assumption, *a priori*, that topography is a key control on flood susceptibility. To test if flood-driven failure of coastal (and other floodplain) road networks is fundamentally a function of topography at critical nodes will require sustained observation of real settings (e.g., Plane et al., 2019). But if borne out, then this work demonstrates how specific nodes, or sets of nodes, in a road network might be targeted in planning strategies for climate adaptation at local scales – especially where resources for adaptation are limited, and specific actions (e.g., raising a road surface over a given distance) may have noticeable effect on the impact of increasingly frequent disturbances.

Local actions at critical nodes in road networks – and other networked infrastructure – are important because, as our results illustrate, the local failure of a critical node triggers a nonlocal failure of the larger network in which it sits. Climate-driven, local disruptions with nonlocal consequences represent a vital concern not only for physical networks of critical infrastructure (Arrighi et al., 2021; Hummel et al., 2018; Li et al., 2015), but also for the emplacement of hazard defenses, which can displace or amplify hazard impacts alongshore (Ells & Murray, 2012; Lazarus et al., 2016; Wang et al., 2018) or downstream (Tobin, 1995). Our analysis suggests that if the critical node of a road network is elevated, for example, by a local intervention that rearranges the three-dimensional network topology, then a different node elsewhere in the network will become the new critical junction. However, if the new critical node corresponds to a significantly lower annual exceedance probability, then the functional susceptibility of the network will have improved in kind – as long as other interventions, such as hazard defenses, do not likewise displace flooding impacts in unintentionally confounding ways.

Broadly, our findings contribute to a diverse and rapidly expanding body of work concerning climate-driven impacts to infrastructure (Faturechi and Miller-Hooks, 2015; Jaroszweski et al., 2014; Markolf et al., 2019; Neumann et al., 2021; Wang et al., 2020), and pertain to forward-looking discourse on sustainable urban systems, including calls for "developing new data and methods to understand current drivers and interactions among natural, human-built, and social systems in urban areas as they impact multiple sustainability outcomes across scales" (ACERE, 2018). Development of simple diagnostics for infrastructure susceptibility in built environments with high exposure to natural hazard should only become more promising with improved accessibility to high-resolution geospatial data for natural and human systems. Specifically, our results can contribute to forward-looking predictions of barrier island dynamics. Future work can incorporate thresholds for road network functioning into barrier island models. Numerical models could include human actions and management strategies that acknowledge thresholds in infrastructure functioning and incorporate hazard-mitigation practices that aim to protect infrastructure. We anticipate that feedbacks between sediment dynamics and infrastructure will also contribute to future barrier island dynamics.

Acknowledgements

EBG and EDL thank Katherine Anarde, Beth Sciaudone, Kenny Ells, and Dylan McNamara for fruitful discussions. The authors gratefully acknowledge support from a Southampton Marine and Maritime Institute Doctoral Studentship (to SA), The Leverhulme Trust (RPG-2018-282, to EDL and EBG), and an Early-Career Research Fellowship from the Gulf Research Program of the National Academies of Sciences, Engineering, and Medicine (to EBG). The content is solely the responsibility of the authors and does not necessarily represent the official views of the Gulf Research Program of the National Academies of Sciences, Engineering, and Medicine.

Data and code availability

All datasets and analytical code used in this study are publicly available from the cited sources listed in the manuscript text.

Our code to extract and analyze road networks and topography is available on Github – https://github.com/envidynxlab/Networks_Barriers – and will be given a DOI upon the completion of the review process.

This manuscript relies on open data, specifically CUDEM (https://coast.noaa.gov/htdata/raster2/elevation/NCEI_ninth_Topobathy_2014_8483/), OSM (https://www.openstreetmap.org; accessed programmatically via Boeing, 2017), and Barrier Island shapefiles (Mulhern et al., 2021).

Author Contributions (CRediT contributor roles)

SA – investigation, methodology, formal analysis, writing, data curation; *EBG* – conceptualization, investigation, methodology, formal analysis, writing, funding acquisition; *EDL* – conceptualization, investigation, methodology, formal analysis, writing, supervision, project administration, funding acquisition.

References

Abdulla, B., & Birgisson, B. (2021). Characterization of vulnerability of road networks to random and nonrandom disruptions using network percolation approach. *Journal of Computing in Civil Engineering*, 35(1), 04020054.

Albert, R., & Barabási, A. L. (2002). Statistical mechanics of complex networks. *Reviews of Modern Physics*, *74*(1), 47–97.

Advisory Committee for Environmental Research and Education (ACERE). (2018). *Sustainable urban systems: Articulating a long-term convergence research agenda.* NSF Advisory Committee for Environmental Research and Education report, Sustainable Urban Systems Subcommittee. Available via https://www.nsf.gov/ere/ereweb/ac-ere/sustainable-urban-systems.pdf. Accessed November 2021.

Amante, C., Stroker, K., Love, M., Stiller, M., Carignan, N., & Arcos, N. (2021). Coastal digital elevation models (DEMs) to support storm surge inundation modelling. Presented at 101st American Meterological Society Annual Meeting (virtual): https://ams.confex.com/ams/101ANNUAL/meetingapp.cgi/Paper/380075

Anarde, K. A., Kameshwar, S., Irza, J. N., Nittrouer, J. A., Lorenzo-Trueba, J., Padgett, J. E., et al. (2018). Impacts of hurricane storm surge on infrastructure vulnerability for an evolving coastal landscape. *Natural Hazards Review*, *19*(1), 04017020.

Apel, H., Thieken, A. H., Merz, B., & Blöschl, G. (2004). Flood risk assessment and associated uncertainty. *Natural Hazards and Earth System Sciences*, *4*(2), 295–308.

Apel, H., Thieken, A. H., Merz, B., & Blöschl, G. (2006). A probabilistic modelling system for assessing flood risks. *Natural Hazards*, *38*(1), 79–100.

Armstrong, S. B., & Lazarus, E. D. (2019). Masked shoreline erosion at large spatial scales as a collective effect of beach nourishment. *Earth's Future*, *7*(2), 74–84.

Armstrong, S. B., Lazarus, E. D., Limber, P. W., Goldstein, E. B., Thorpe, C., & Ballinger, R. C. (2016). Indications of a positive feedback between coastal development and beach nourishment. *Earth's Future*, *4*(12), 626–635.

Arrighi, C., Pregnolato, M., & Castelli, F. (2021). Indirect flood impacts and cascade risk across interdependent linear infrastructures. *Natural Hazards and Earth System Sciences*, *21*(6), 1955–1969.

Balomenos, G. P., Hu, Y., Padgett, J. E., & Shelton, K. (2019). Impact of coastal hazards on residents' spatial accessibility to health services. *Journal of Infrastructure Systems*, *25*(4), 04019028.

Buchanan, M. K., Oppenheimer, M., & Kopp, R. E. (2017). Amplification of flood frequencies with local sea level rise and emerging flood regimes. *Environmental Research Letters*, *12*(6), 064009.

Callaway, D. S., Newman, M. E., Strogatz, S. H., & Watts, D. J. (2000). Network robustness and fragility: Percolation on random graphs. *Physical Review Letters*, *85*(25), 5468.

Chang, S. E. (2016). Socioeconomic impacts of infrastructure disruptions. In *Oxford Research Encyclopedias: Natural Hazard Science*. Oxford University Press. https://doi.org/10.1093/acrefore/9780199389407.013.66.

Cheng, L., & AghaKouchak, A. (2014). Nonstationary precipitation intensity-duration-frequency curves for infrastructure design in a changing climate. *Scientific Reports*, *4*(1), 1–6.

Coles, S. (2001). *An introduction to statistical modeling of extreme values*. London: Springer-Verlag.

Cooperative Institute for Research in Environmental Sciences (CIRES) at the University of Colorado, Boulder. (2014). Continuously Updated Digital Elevation Model (CUDEM) – 1/9 Arc-Second Resolution Bathymetric-Topographic Tiles. NOAA National Centers for Environmental Information. https://doi.org/10.25921/ds9v-ky35. Accessed November 2021.

Darestani, Y. M., Webb, B., Padgett, J. E., Pennison, G., & Fereshtehnejad, E. (2021). Fragility analysis of coastal roadways and performance assessment of coastal transportation systems subjected to storm hazards. *Journal of Performance of Constructed Facilities*, *35*(6), 04021088.

Dave, R., Subramanian, S. S., & Bhatia, U. (2021). Extreme precipitation induced concurrent events trigger prolonged disruptions in regional road networks. *Environmental Research Letters*, *16*(10), 104050.

de Bruijn, K. M., Maran, C., Zygnerski, M., Jurado, J., Burzel, A., Jeuken, C., & Obeysekera, J. (2019). Flood resilience of critical infrastructure: Approach and method applied to Fort Lauderdale, Florida. *Water*, *11*(3), 517.

Dolan, R., Hayden, B., & Lins, H. (1980). Barrier Islands: The natural processes responsible for the evolution of barrier islands and for much of their recreational and aesthetic appeal also make them hazardous places for humans to live. *American Scientist*, *68*(1), 16–25.

Dolan, R., & Lins, H. F. (2000). The Outer Banks of North Carolina. US Geological Survey Professional Paper 1177–B, US Government Printing Office.

Dong, S., Esmalian, A., Farahmand, H., & Mostafavi, A. (2020a). An integrated physical-social analysis of disrupted access to critical facilities and community service-loss tolerance in urban flooding. *Computers, Environment and Urban Systems*, *80*, 101443.

Dong, S., Mostafizi, A., Wang, H., Gao, J., & Li, X. (2020b). Measuring the topological robustness of transportation networks to disaster-induced failures: A percolation approach. *Journal of Infrastructure Systems*, *26*(2), 04020009.

Douglas, E. M., Kirshen, P. H., Bosma, K., Watson, C., Miller, S., & McArthur, K. (2016). Simulating the impacts and assessing the vulnerability of the central artery/tunnel system to sea level rise and increased coastal flooding. *Journal of Extreme Events*, *3*(04), 1650013.

Ells, K., & Murray, A. B. (2012). Long-term, non-local coastline responses to local shoreline stabilization. *Geophysical Research Letters*, *39*(19).

Emanuelsson, M. A. E., McIntyre, N., Hunt, C. F., Mawle, R., Kitson, J., & Voulvoulis, N. (2014). Flood risk assessment for infrastructure networks. *Journal of Flood Risk Management*, *7*(1), 31–41.

Evans, B., Chen, A. S., Djordjević, S., Webber, J., Gómez, A. G., & Stevens, J. (2020). Investigating the Effects of Pluvial Flooding and Climate Change on Traffic Flows in Barcelona and Bristol. *Sustainability*, *12*(6), 2330.

Ezer, T., & Atkinson, L. P. (2014). Accelerated flooding along the US East Coast: On the impact of sea-level rise, tides, storms, the Gulf Stream, and the North Atlantic Oscillations. *Earth's Future*, *2*(8), 362–382.

Fant, C., Jacobs, J. M., Chinowsky, P., Sweet, W., Weiss, N., Sias, J. E., et al. (2021). Mere nuisance or growing threat? The physical and economic impact of high tide flooding on US road networks. *Journal of Infrastructure Systems*, *27*(4), 04021044.

Faturechi, R., & Miller-Hooks, E. (2015). Measuring the performance of transportation infrastructure systems in disasters: A comprehensive review. *Journal of Infrastructure Systems*, *21*(1), 04014025.

Frazier, T. G., Thompson, C. M., Dezzani, R. J., & Butsick, D. (2013). Spatial and temporal quantification of resilience at the community scale. *Applied Geography*, *42*, 95–107.

Godschalk, D. R., Brower, D. J., & Beatley, T. (1989). *Catastrophic coastal storms: Hazard mitigation and development management*. Duke University Press.

Gopalakrishnan, S., Landry, C. E., Smith, M. D., & Whitehead, J. C. (2016). Economics of coastal erosion and adaptation to sea level rise. *Annual Review of Resource Economics*, *8*, 119–139.

Gopalakrishnan, S., Smith, M. D., Slott, J. M., & Murray, A. B. (2011). The value of disappearing beaches: A hedonic pricing model with endogenous beach width. *Journal of Environmental Economics and Management*, *61*(3), 297–310.

Habel, S., Fletcher, C. H., Rotzoll, K., & El-Kadi, A. I. (2017). Development of a model to simulate groundwater inundation induced by sea-level rise and high tides in Honolulu, Hawaii. *Water Research*, *114*, 122–134.

Habel, S., Fletcher, C. H., Anderson, T. R., & Thompson, P. R. (2020). Sea-level rise induced multi-mechanism flooding and contribution to urban infrastructure failure. *Scientific Reports*, *10*(1), 1–12.

Hackl, J., Lam, J. C., Heitzler, M., Adey, B. T., & Hurni, L. (2018). Estimating network related risks: A methodology and an application in the transport sector. *Natural Hazards and Earth System Sciences*, *18*(8), 2273–2293.

Hagberg, A., Swart, P., & S Chult, D. (2008). *Exploring network structure, dynamics, and function using NetworkX* (No. LA-UR-08-05495; LA-UR-08-5495). Los Alamos National Lab.(LANL), Los Alamos, NM, USA.

Haigh, I. D., MacPherson, L. R., Mason, M. S., Wijeratne, E. M. S., Pattiaratchi, C. B., Crompton, R. P., & George, S. (2014). Estimating present day extreme water level exceedance probabilities around the coastline of Australia: tropical cyclone-induced storm surges. *Climate Dynamics*, *42*(1-2), 139-157.

Hardin, E., Mitasova, H., & Overton, M. (2012). GIS-based analysis of storm vulnerability change at Pea Island, NC. *Coastal Engineering Proceedings*, *1*(33), https://doi.org/10.9753/icce.v33.management.75

Harris, C. R., Millman, K. J., van der Walt, S. J., Gommers, R., Virtanen, P., Cournapeau, D., et al. (2020). Array programming with NumPy. *Nature*, *585*(7825), 357–362.

Hiatt, M., Addink, E.A. & Kleinhans, M.G. (2021). Connectivity and directionality in estuarine channel networks. *Earth Surface Processes and Landforms*, https://doi.org/10.1002/esp.5286

Hino, M., Belanger, S. T., Field, C. B., Davies, A. R., & Mach, K. J. (2019). High-tide flooding disrupts local economic activity. *Science Advances*, *5*(2), eaau2736.

Holme, P., Kim, B. J., Yoon, C. N., & Han, S. K. (2002). Attack vulnerability of complex networks. *Physical Review E*, *65*(5), 056109.

Housego, R., Raubenheimer, B., Elgar, S., Cross, S., Legner, C., & Ryan, D. (2021). Coastal flooding generated by ocean wave-and surge-driven groundwater fluctuations on a sandy barrier island. *Journal of Hydrology*, *603*, 126920.

Hummel, M. A., Berry, M. S., & Stacey, M. T. (2018). Sea level rise impacts on wastewater treatment systems along the US coasts. *Earth's Future*, *6*(4), 622–633.

Iyer, S., Killingback, T., Sundaram, B., & Wang, Z. (2013). Attack robustness and centrality of complex networks. *PloS One*, *8*(4), e59613.

Jacobs, J. M., Cattaneo, L. R., Sweet, W., & Mansfield, T. (2018). Recent and future outlooks for nuisance flooding impacts on roadways on the US East Coast. *Transportation Research Record*, *2672*(2), 1–10.

Jamakovic, A., & Uhlig, S. (2008). On the relationships between topological measures in real-world networks. *Networks & Heterogeneous Media*, *3*(2), 345–359.

Jaroszweski, D., Hooper, E., & Chapman, L. (2014). The impact of climate change on urban transport resilience in a changing world. *Progress in Physical Geography*, *38*(4), 448–463.

Jenelius, E., & Mattsson, L. G. (2012). Road network vulnerability analysis of area-covering disruptions: A grid-based approach with case study. *Transportation Research Part A: policy and practice*, *46*(5), 746–760.

Johansen, C., & Tien, I. (2018). Probabilistic multi-scale modeling of interdependencies between critical infrastructure systems for resilience. *Sustainable and Resilient Infrastructure*, *3*(1), 1–15.

Kasmalkar, I. G., Serafin, K. A., Miao, Y., Bick, I. A., Ortolano, L., Ouyang, D., & Suckale, J. (2020). When floods hit the road: Resilience to flood-related traffic disruption in the San Francisco Bay Area and beyond. *Science Advances*, *6*(32), eaba2423.

Kelleher, C., & McPhillips, L. (2020). Exploring the application of topographic indices in urban areas as indicators of pluvial flooding locations. *Hydrological Processes*, *34*(3), 780–794.

Kermanshah, A., & Derrible, S. (2017). Robustness of road systems to extreme flooding: using elements of GIS, travel demand, and network science. *Natural Hazards*, *86*(1), 151–164.

Kirezci, E., Young, I. R., Ranasinghe, R., Muis, S., Nicholls, R. J., Lincke, D., & Hinkel, J. (2020). Projections of global-scale extreme sea levels and resulting episodic coastal flooding over the 21st Century. *Scientific Reports*, *10*(1), 1–12.

Kirkley, A., Barbosa, H., Barthelemy, M., & Ghoshal, G. (2018). From the betweenness centrality in street networks to structural invariants in random planar graphs. *Nature Communications*, *9*(1), 1–12.

Koks, E. E., Rozenberg, J., Zorn, C., Tariverdi, M., Vousdoukas, M., Fraser, S. A., et al. (2019). A global multi-hazard risk analysis of road and railway infrastructure assets. *Nature Communications*, *10*(1), 1–11.

Krynock, L. W., Shelden, J. G., & Martin, J. D. (2005). Highway Vulnerability Along NC 12 – Ocracoke Island, North Carolina. Presented at Solutions to Coastal Disasters Conference 2005, 423–432, https://doi.org/10.1061/40774(176)43

Lazarus, E. D., & Goldstein, E. B. (2019). Is there a bulldozer in your model? *Journal of Geophysical Research: Earth Surface*, *124*(3), 696–699.

Lazarus, E. D., Ellis, M. A., Murray, A. B., & Hall, D. M. (2016). An evolving research agenda for human–coastal systems. *Geomorphology*, 256, 81–90.

Lazarus, E. D., Goldstein, E. B., Taylor, L. A., & Williams, H. E. (2021). Comparing patterns of hurricane washover into built and unbuilt environments. *Earth's Future*, *9*(3), e2020EF001818.

Lazarus, E. D., Limber, P. W., Goldstein, E. B., Dodd, R., & Armstrong, S. B. (2018). Building back bigger in hurricane strike zones. *Nature Sustainability*, *1*(12), 759–762.

Li, D., Fu, B., Wang, Y., Lu, G., Berezin, Y., Stanley, H. E., & Havlin, S. (2015). Percolation transition in dynamical traffic network with evolving critical bottlenecks. *Proceedings of the National Academy of Sciences USA*, *112*(3), 669–672.

Markolf, S. A., Hoehne, C., Fraser, A., Chester, M. V., & Underwood, B. S. (2019). Transportation resilience to climate change and extreme weather events–Beyond risk and robustness. *Transport Policy*, *74*, 174–186.

Mattsson, L. G., & Jenelius, E. (2015). Vulnerability and resilience of transport systems–A discussion of recent research. *Transportation Research Part A: Policy and Practice*, *81*, 16–34.

McNamara, D. E., & Keeler, A. (2013). A coupled physical and economic model of the response of coastal real estate to climate risk. *Nature Climate Change*, *3*(6), 559–562.

McNamara, D. E., & Lazarus, E. D. (2018). Barrier islands as coupled human–landscape systems. In Moore, L. J. & Murray, A. B. (Eds.) *Barrier dynamics and response to changing climate* (pp. 363-383). Springer, Cham.

McNamara, D. E., & Werner, B. T. (2008a). Coupled barrier island–resort model: 1. Emergent instabilities induced by strong human-landscape interactions. *Journal of Geophysical Research: Earth Surface*, 113(F1), 113, F01016, doi:10.1029/2007JF000840.

McNamara, D. E., & Werner, B. T. (2008b). Coupled barrier island–resort model: 2. Tests and predictions along Ocean City and Assateague Island National Seashore, Maryland. *Journal of Geophysical Research: Earth Surface*, 113(F1), F01017, doi:10.1029/2007JF000841.

McNamara, D. E., Gopalakrishnan, S., Smith, M. D., & Murray, A. B. (2015). Climate adaptation and policy-induced inflation of coastal property value. *PloS One*, *10*(3), e0121278.

McNamara, D. E., Murray, A. B., and Smith, M. D. (2011), Coastal sustainability depends on how economic and coastline responses to climate change affect each other, *Geophysical Research Letters*, *38*, L07401, doi:10.1029/2011GL047207.

Miselis, J. L., & Lorenzo‐Trueba, J. (2017). Natural and human‐induced variability in barrier‐island response to sea level rise. *Geophysical Research Letters*, *44*(23), 11–922.

Moftakhari, H. R., AghaKouchak, A., Sanders, B. F., Feldman, D. L., Sweet, W., Matthew, R. A., & Luke, A. (2015). Increased nuisance flooding along the coasts of the United States due to sea level rise: Past and future. *Geophysical Research Letters*, *42*(22), 9846–9852.

Moftakhari, H. R., AghaKouchak, A., Sanders, B. F., & Matthew, R. A. (2017). Cumulative hazard: The case of nuisance flooding. *Earth's Future*, *5*(2), 214–223.

Moftakhari, H. R., AghaKouchak, A., Sanders, B. F., Allaire, M., & Matthew, R. A. (2018). What is nuisance flooding? Defining and monitoring an emerging challenge. *Water Resources Research*, *54*, 4218–4227. https://doi.org/10.1029/2018WR022828

Moreira, A. A., Andrade Jr, J. S., Herrmann, H. J., & Indekeu, J. O. (2009). How to make a fragile network robust and vice versa. *Physical Review Letters*, *102*(1), 018701.

Muis, S., Apecechea, M. I., Dullaart, J., de Lima Rego, J., Madsen, K. S., Su, J., et al. (2020). A high-resolution global dataset of extreme sea levels, tides, and storm surges, including future projections. *Frontiers in Marine Science*, *7*, 263.

Mulhern, J. S., Johnson, C. L., & Martin, J. M. (2021). Data for: Is barrier island morphology a function of tidal and wave regime? [Dataset] Hive. https://doi.org/10.7278/S50d-5pzj-r9vr.

Mulhern, J. S., Johnson, C. L., & Martin, J. M. (2017). Is barrier island morphology a function of tidal and wave regime? *Marine Geology*, 387, 74–84.

Najafi, M. R., Zhang, Y., & Martyn, N. (2021). A flood risk assessment framework for interdependent infrastructure systems in coastal environments. *Sustainable Cities and Society*, *64*, 102516. https://doi.org/10.1016/j.scs.2020.102516

Najibi, N., & Devineni, N. (2018). Recent trends in the frequency and duration of global floods. *Earth System Dynamics*, *9*(2), 757-783.

Neumann, J. E., Chinowsky, P., Helman, J., Black, M., Fant, C., Strzepek, K., & Martinich, J. (2021). Climate effects on US infrastructure: the economics of adaptation for rail, roads, and coastal development. *Climatic Change*, *167*(3), 1–23.

Newman, M. 2010. *Networks: An introduction*. Oxford University Press.

Nicholson, A., & Du, Z. P. (1997). Degradable transportation systems: an integrated equilibrium model. *Transportation Research Part B: Methodological*, *31*(3), 209–223.

Nordstrom, K. F. (1994). Beaches and dunes of human-altered coasts. *Progress in Physical Geography*, *18*(4), 497–516.

Nordstrom, K. F. (2004). *Beaches and dunes of developed coasts*. Cambridge University Press.

Nordstrom, K. F., & Jackson, N. L. (1995). Temporal scales of landscape change following storms on a human-altered coast, New Jersey, USA. *Journal of Coastal Conservation*, *1*(1), 51–62.

National Oceanic and Atmospheric Administration (NOAA) (2013). National Coastal Population Report: Population Trends from 1970 to 2020. Available via https://coast.noaa.gov/digitalcoast/training/population-report.html. Accessed August 2021.

Passalacqua, P. (2017). The Delta Connectome: A network-based framework for studying connectivity in river deltas. *Geomorphology*, *277*, 50–62.

Plane, E., Hill, K., & May, C. (2019). A rapid assessment method to identify potential groundwater flooding hotspots as sea levels rise in coastal cities. *Water*, *11*(11), 2228.

Pearson, S. G., van Prooijen, B. C., Elias, E. P., Vitousek, S., & Wang, Z. B. (2020). Sediment connectivity: a framework for analyzing coastal sediment transport pathways. *Journal of Geophysical Research: Earth Surface*, *125*(10), e2020JF005595.

Pezza, D. A., & White, J. M. (2021). Impact of the duration of coastal flooding on infrastructure. *Public Works Management & Policy*, *26*(2), 144–163.

Porta, S., Crucitti, P., & Latora, V. (2006). The network analysis of urban streets: A dual approach. *Physica A: Statistical Mechanics and its Applications*, *369*(2), 853–866.

Praharaj, S., Chen, T. D., Zahura, F. T., Behl, M., & Goodall, J. L. (2021). Estimating impacts of recurring flooding on roadway networks: a Norfolk, Virginia case study. *Natural Hazards*, *107*, 2363–2387. https://doi.org/10.1007/s11069-020-04427-5

Pregnolato, M., Ford, A., Glenis, V., Wilkinson, S., & Dawson, R. (2017). Impact of climate change on disruption to urban transport networks from pluvial flooding. *Journal of Infrastructure Systems*, *23*(4), 04017015.

Rogers, L. J., Moore, L. J., Goldstein, E. B., Hein, C. J., Lorenzo-Trueba, J., & Ashton, A. D. (2015). Anthropogenic controls on overwash deposition: Evidence and consequences. *Journal of Geophysical Research: Earth Surface*, *120*(12), 2609–2624.

Rotzoll, K., & Fletcher, C. H. (2013). Assessment of groundwater inundation as a consequence of sea-level rise. *Nature Climate Change*, *3*(5), 477–481.

Sadler, J. M., Haselden, N., Mellon, K., Hackel, A., Son, V., Mayfield, J., et al. (2017). Impact of sea-level rise on roadway flooding in the Hampton Roads region, Virginia. *Journal of Infrastructure Systems*, *23*(4), 05017006.

Schneider, C. M., Moreira, A. A., Andrade, J. S., Havlin, S., & Herrmann, H. J. (2011). Mitigation of malicious attacks on networks. *Proceedings of the National Academy of Sciences USA*, *108*(10), 3838–3841.

Serafin, K. A., Ruggiero, P., & Stockdon, H. F. (2017). The relative contribution of waves, tides, and nontidal residuals to extreme total water levels on US West Coast sandy beaches. *Geophysical Research Letters*, *44*(4), 1839–1847. https://doi.org/10.1002/2016gl071020

Singh, P., Sinha, V. S. P., Vijhani, A., & Pahuja, N. (2018). Vulnerability assessment of urban road network from urban flood. *International Journal of Disaster Risk Reduction*, *28*, 237–250.

Smith, M. D., Slott, J. M., McNamara, D., & Murray, A. B. (2009). Beach nourishment as a dynamic capital accumulation problem. *Journal of Environmental Economics and Management*, *58*(1), 58–71.

Spanger-Siegfried, E., Fitzpatrick, M., & Dahl, K. (2014). Encroaching tides: How sea level rise and tidal flooding threaten US East and Gulf Coast communities over the next 30 years. Union of Concerned Scientists. Cambridge, Massachusetts. Available via https://www.ucsusa.org/resources/encroaching-tides. Accessed November 2021.

Stutz, M. L., & Pilkey, O. H. (2011). Open-ocean barrier islands: global influence of climatic, oceanographic, and depositional settings. *Journal of Coastal Research*, *27*(2), 207–222.

Suarez, P., Anderson, W., Mahal, V., & Lakshmanan, T. R. (2005). Impacts of flooding and climate change on urban transportation: A systemwide performance assessment of the Boston Metro Area. *Transportation Research Part D: transport and environment*, *10*(3), 231–244.

Sweet, W. V., & Park, J. (2014). From the extreme to the mean: Acceleration and tipping points of coastal inundation from sea level rise. *Earth's Future*, *2*(12), 579–600.

Sweet, W., Park, J., Marra, J., Zervas, C., & Gill, S. (2014). Sea level rise and nuisance flood frequency changes around the United States. NOAA Technical Report NOS CO-OPS 073. Available via https://tidesandcurrents.noaa.gov/publications/NOAA_Technical_Report_NOS_COOPS_073.pdf. Accessed November 2021.

Tadesse, M. G., & Wahl, T. (2021). A database of global storm surge reconstructions. *Scientific Data*, *8*(1), 1–10.

Taherkhani, M., Vitousek, S., Barnard, P. L., Frazer, N., Anderson, T. R., & Fletcher, C. H. (2020). Sea-level rise exponentially increases coastal flood frequency. *Scientific Reports*, *10*(1), 1–17.

Tebaldi, C., Strauss, B. H., & Zervas, C. E. (2012). Modelling sea level rise impacts on storm surges along US coasts. *Environmental Research Letters*, *7*(1), 014032.

Tejedor, A., Longjas, A., Passalacqua, P., Moreno, Y., & Foufoula-Georgiou, E. (2018). Multiplex networks: A framework for studying multiprocess multiscale connectivity via coupled-network theory with an application to river deltas. *Geophysical Research Letters*, *45*(18), 9681–9689.

Tian, J., Yu, M., Ren, C., & Lei, Y. (2019). Network-scape metric analysis: a new approach for the pattern analysis of urban road networks. *International Journal of Geographical Information Science*, *33*(3), 537–566.

Tobin, G. A. (1995). The levee love affair: a stormy relationship? *JAWRA Journal of the American Water Resources Association*, *31*(3), 359–367.

Velasquez-Montoya, L., Sciaudone, E. J., Smyre, E., & Overton, M. F. (2021). Vulnerability indicators for coastal roadways based on barrier island morphology and shoreline change predictions. *Natural Hazards Review*, *22*(2), 04021003.

Versini, P. A., Gaume, E., & Andrieu, H. (2010). Assessment of the susceptibility of roads to flooding based on geographical information–test in a flash flood prone area (the Gard region, France). *Natural Hazards and Earth System Sciences*, *10*(4), 793–803.

Virtanen, P., Gommers, R., Oliphant, T. E., Haberland, M., Reddy, T., Cournapeau, D., et al. (2020). SciPy 1.0: Fundamental algorithms for scientific computing in Python. *Nature Methods*, *17*, 261–272. https://doi.org/10.1038/s41592-019-0686-2

Vitousek, S., Barnard, P. L., Fletcher, C. H., Frazer, N., Erikson, L., & Storlazzi, C. D. (2017). Doubling of coastal flooding frequency within decades due to sea-level rise. *Scientific Reports*, *7*(1), 1–9.

Wahl, T., Haigh, I. D., Nicholls, R. J., Arns, A., Dangendorf, S., Hinkel, J., & Slangen, A. B. (2017). Understanding extreme sea levels for broad-scale coastal impact and adaptation analysis. *Nature Communications*, *8*(1), 1–12.

Wang, R. Q., Stacey, M. T., Herdman, L. M. M., Barnard, P. L., & Erikson, L. (2018). The influence of sea level rise on the regional interdependence of coastal infrastructure. *Earth's Future*, *6*(5), 677–688.

Wang, T., Qu, Z., Yang, Z., Nichol, T., Clarke, G., & Ge, Y. E. (2020). Climate change research on transportation systems: Climate risks, adaptation and planning. *Transportation Research Part D: Transport and Environment, 88*, 102553.

Wang, W., Yang, S., Stanley, H. E., & Gao, J. (2019). Local floods induce large-scale abrupt failures of road networks. *Nature Communications*, *10*(1), 1–11.

Williams, Z. C., McNamara, D. E., Smith, M. D., Murray, A. B., & Gopalakrishnan, S. (2013). Coupled economic-coastline modeling with suckers and free riders. *Journal of Geophysical Research: Earth Surface*, *118*(2), 887–899.

Woodworth, P. L., Hunter, J. R., Marcos, M., Caldwell, P., Menéndez, M., & Haigh, I. (2016). Towards a global higher-frequency sea level dataset. *Geoscience Data Journal*, *3*(2), 50–59.

Zervas, C. (2013). Extreme water levels of the United States 1893–2010. NOAA Technical Report NOS CO-OPS 067, Silver Spring, Maryland. Available via https://tidesandcurrents.noaa.gov/publications/NOAA_Technical_Report_NOS_COOPS_067a.pdf. Accessed October 2021.

Zhang, K., & Leatherman, S. (2011). Barrier island population along the US Atlantic and Gulf Coasts. *Journal of Coastal Research*, *27*(2), 356–363.